The influence of radiatively active water ice clouds on the Martian climate

J.-B. Madeleine,[1,2] F. Forget,[1] E. Millour,[1] T. Navarro,[1] and A. Spiga[1]

Received 13 August 2012; revised 24 October 2012; accepted 2 November 2012; published 12 December 2012.

[1] Radiatively active water ice clouds (RAC) play a key role in shaping the thermal structure of the Martian atmosphere. In this paper, RAC are implemented in the LMD Mars Global Climate Model (GCM) and the simulated temperatures are compared to Thermal Emission Spectrometer observations over a full year. RAC change the temperature gradients and global dynamics of the atmosphere and this change in dynamics in turn implies large-scale adiabatic temperature changes. Therefore, clouds have both a direct and indirect effect on atmospheric temperatures. RAC successfully reduce major GCM temperature biases, especially in the regions of formation of the aphelion cloud belt where a cold bias of more than 10 K is corrected. Departures from the observations are however seen in the polar regions, and highlight the need for better modeling of cloud formation and evolution. **Citation:** Madeleine, J.-B., F. Forget, E. Millour, T. Navarro, and A. Spiga (2012), The influence of radiatively active water ice clouds on the Martian climate, *Geophys. Res. Lett.*, *39*, L23202, doi:10.1029/2012GL053564.

1. Introduction

[2] Over the last decade, it has become clear that the radiative effect of water ice clouds plays an essential role in the climate of Mars. The effect of radiatively active clouds (hereafter called RAC) was first modeled using the GFDL Mars Global Climate Model (MGCM) by *Rodin et al.* [1999] and further brought out by *Schofield et al.* [1997] and *Magalhães et al.* [1999] who found a strong thermal inversion between 10 and 16 km in the temperature profile retrieved during the EDL (Entry, Descent and Landing) of Pathfinder. This inversion was further analyzed by *Haberle et al.* [1999] and *Colaprete et al.* [1999] and attributed to infrared emissions by clouds, but the temperatures were later found to be too warm compared to other observations [*Clancy et al.*, 2000] and possibly biased at these altitudes [*Withers and Smith*, 2006]. Other inversions were later discovered in the equatorial regions during the $L_s = 145°–155°$ period in the radio occultations of MGS (Mars Global Surveyor) and successfully reproduced by implementing the radiative effect of clouds in the GFDL/MGCM [*Hinson and Wilson*, 2004]. Further characterization of the radiative effect of clouds was made by *Wilson et al.* [2008] who analyzed the reanalysis made by *Montabone et al.* [2006] of the TES temperature retrievals (Thermal Emission Spectrometer [*Conrath et al.*, 2000; *Smith*, 2004]). They showed that the atmospheric temperatures in the equatorial region can only be fully explained by taking into account the radiative effect of clouds. *Wilson et al.* [2007] also interpreted a warm bias in the nighttime surface temperatures retrieved by TES as being due to the thermal emission of water ice clouds. More recently, *Wilson* [2011] also characterized low-level tropical clouds and similar temperature inversions throughout the aphelion season ($L_s = 20°–130°$) in the Mars Climate Sounder data.

[3] In this paper, we analyze the impact of RAC on the global climate of Mars and compare simulated temperatures to observations over one full Martian year. We start by describing the implementation of the radiative effect of water ice clouds in the LMD (Laboratoire de Météorologie Dynamique) MGCM in section 2, then analyze the effects of clouds on a typical temperature profile in section 3 and finally compare the simulations of our 3D global climate model to the TES observations in section 4.

2. Implementation

2.1. Cloud Formation

[4] The version of the model used in this paper builds on the work published in *Madeleine et al.* [2011]. It uses a new representation of the dust cycle as well as the so-called "semi-interactive" dust transport scheme described therein. The cloud scheme is similar to the one described in *Montmessin et al.* [2004], except that the amount and size of dust nuclei are computed by the dust transport scheme, instead of following analytical profiles [*Montmessin et al.*, 2004, paragraph 29]. Yet, the fraction of dust particles involved in cloud formation is unknown. We therefore use a tuneable parameter f_{CCN} which is the ratio at a given gridpoint of the total number of dust particles N over the number of condensation nuclei N_c. Increasing this ratio results in larger ice particles because the same amount of water condenses on fewer dust nuclei. Larger ice particles fall faster and tend to decrease the transport of water in the Hadley cell, thereby lowering the overall humidity. The mass mean radius of ice particles is computed by using the following equation [*Montmessin et al.*, 2004]:

$$r_c = \left(\frac{3M_c}{4\pi\rho_i N_c} + r_0^3 \right)^{1/3}, \quad (1)$$

where M_c is the total mass of water ice, ρ_i is the ice density (917 kg m^{-3}), N_c is the number of dust nuclei and r_0 is the

[1]Laboratoire de Météorologie Dynamique, CNRS/UPMC/IPSL, Paris, France.
[2]Now at the Department of Geological Sciences, Brown University, Providence, Rhode Island, USA.

Corresponding author: J.-B. Madeleine, Department of Geological Sciences, Brown University, 324 Brook St., Box 1846, Providence, RI 02912, USA. (jean-baptiste_madeleine@brown.edu)

0094-8276/12/2012GL053564

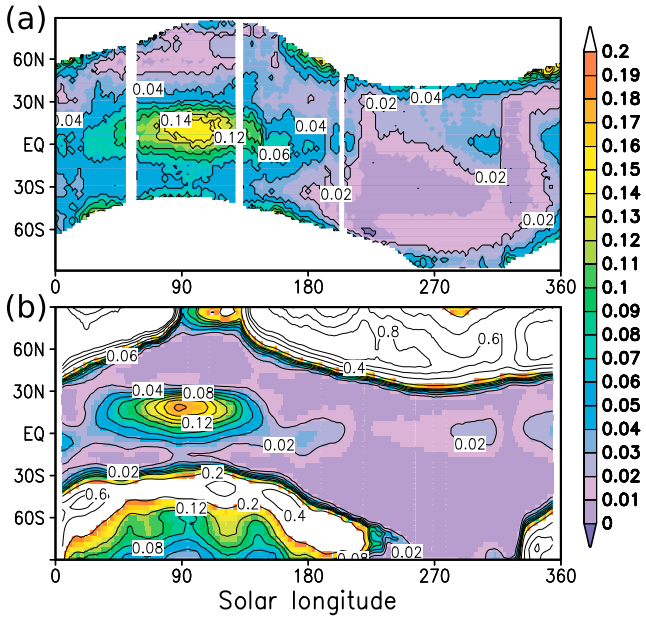

Figure 1. (a) Annual evolution of the zonal mean water ice absorption optical depth at 825 cm^{-1} (12.1 μm) as retrieved by TES. (b) Optical depth simulated by the LMD/MGCM. In both cases, year is MY26 and local time is 2 PM. TES cannot retrieve the water ice opacity in the polar regions, where the GCM predicts thick clouds.

mean radius of dust nuclei. The two variables N_c and r_0 are provided by the dust transport scheme. The mass mean radius of ice particles r_c is then used to compute two different radiuses:

[5] 1. The "sedimentation" radius, $r_{sed} = f_{sed}\, r_c$, where f_{sed} is an enhancement factor that depends on the variance of the size distribution and accounts for the stronger contribution of larger particles to the sedimentation mass flux [see *Montmessin et al.*, 2004, paragraph 30];

[6] 2. The "radiative" effective radius, $r_{rad} = r_c\,(1 + \nu_{rad})$, where ν_{rad} is the effective variance of the lognormal distribution used by the radiative transfer scheme [*Madeleine et al.*, 2011, equation 6].

[7] The radiative effective variance ν_{rad} is set to 0.1 and the two parameters f_{CCN} and f_{sed} are adjusted so that simulated cloud properties are consistent with observations (set to 4.5 and 3, respectively).

2.2. Analyzed Simulations

[8] Simulations are run using the dust opacity acquired by TES/MGS during Martian year 26 (chronology of *Clancy et al.* [2000], with the first Martian year beginning on April 11, 1955). The resolution is 5.625° × 3.75° in the horizontal (64 × 48) with 25 levels in the vertical from 5 m above the ground to ~100 km. The simulated cloud opacity at a wavelength of 12.1 μm is shown in Figure 1b and compared to the observed TES opacity (Figure 1a). Since the focus of this paper is the radiative effect of clouds, cloud opacities and particle sizes were compared to TES and OMEGA observations [*Smith*, 2004; *Wolff and Clancy*, 2003; *Madeleine et al.*, 2012] to ensure that heating rates are accurate.

2.3. Radiative Transfer Scheme

[9] The radiative effect of water ice clouds depends on the single scattering properties of ice particles, which are a function of their size distribution. Scattering properties for different particle sizes are extracted by the LMD/MGCM from precomputed lookup tables which are generated using a Mie code and the optical indices of *Warren* [1984]. At each GCM time step, using the data stored in the lookup tables, scattering properties are integrated over a given size distribution controlled by the cloud particle effective radius r_{rad} predicted by the GCM in each grid box. As mentioned in section 2.1, the radiative effective variance ν_{rad} is kept constant and equal to 0.1. The change in scattering due to the growth of water ice crystals is therefore accounted for in our model (for more details, see section 2.3.2 of *Madeleine et al.* [2011]).

3. Local Radiative Effect of Clouds

[10] Before focusing on global changes induced by RAC, we analyze here the impact of clouds on a typical temperature profile of the equatorial regions. For that purpose, we focus on the temperature changes on the Tharsis plateau (0°N–120°W) for a typical day of the L_s = 90°–120° season (northern summer). Figure 2a shows in contours the difference in temperature profiles T_{active}-$T_{inactive}$ over the course of a day between two GCM simulations: one with RAC

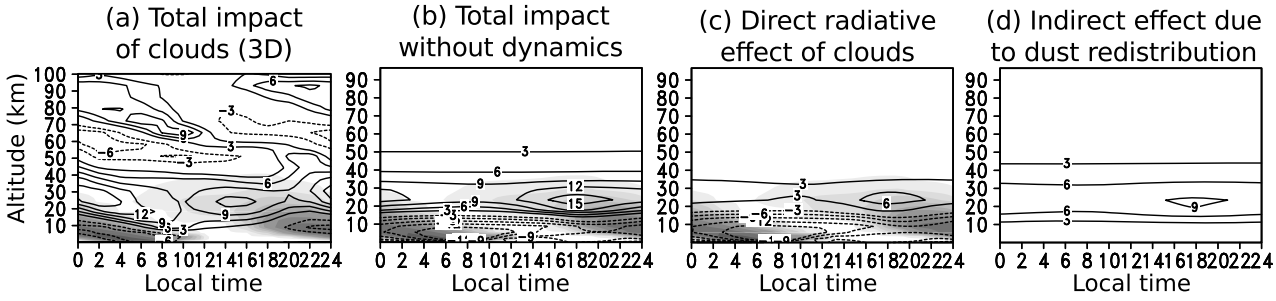

Figure 2. (a) Temperature difference (T_{active}-$T_{inactive}$, contour interval of 3 K) for a typical day of the L_s = 90–120° period over the Tharsis plateau between two 3D simulations, one with radiatively active clouds and the other without. Darker shades indicate higher water ice mole mixing ratio, the maximum value being 250 ppm. (b) Same as Figure 2a, but the 1D version of the climate model is used, and constrained by the dust and water ice profiles of the 3D simulation. (c) Same as Figure 2b, but the dust profile is the same for the two compared simulations. (d) Temperature difference resulting from the change in the vertical distribution of dust only.

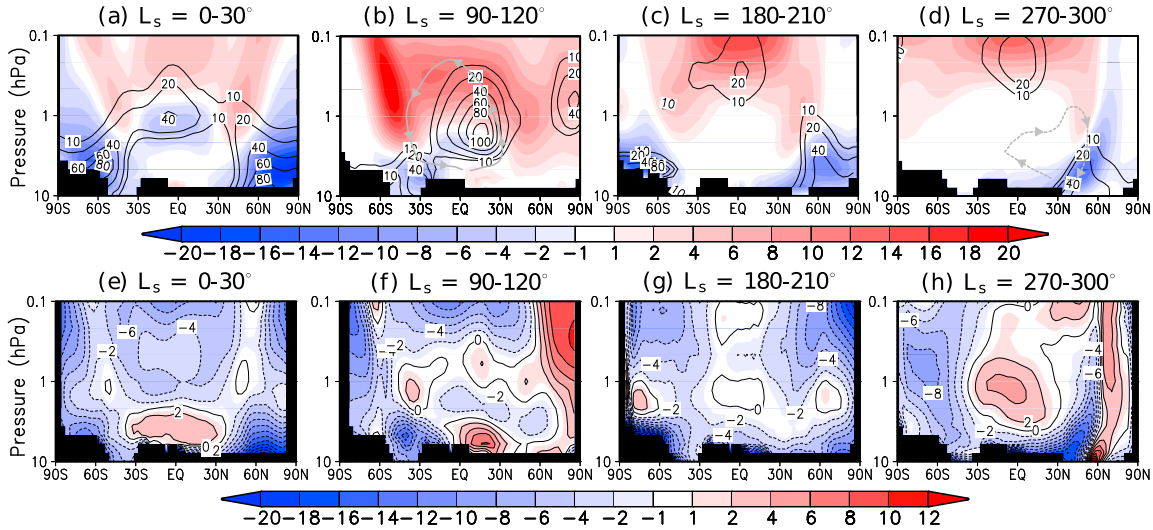

Figure 3. (a–d) Zonal mean temperature difference (in K) between two simulations, one with radiatively active clouds and the other without, for four periods of MY26. Red shade corresponds to a net warming by clouds. Water ice mole mixing ratio is represented by contours, in ppm. The arrowed gray lines in panel b and d were plotted by computing the difference between the two simulations in the meridional mass streamfunction, and represent the 10^9 kg s^{-1} isocontour of this difference (plus or minus, depending on the season). (e–h) Zonal mean temperature difference between a GCM simulation that includes radiatively active clouds and the TES retrievals of *Smith* [2004], for four periods of MY26. Contour interval is 2 K.

and the other without. Black shading indicates the mole mixing ratio of water ice particles, the maximum value being 250 ppm. Water ice clouds change the atmospheric temperature mainly by absorption or emission of thermal infrared radiation. They do not absorb much solar radiation, the single scattering albedo being close to unity at solar wavelengths. Consequently, clouds tend to warm the atmosphere during the day by absorption of the infrared radiation emitted by the surface and to cool the atmosphere during the night by infrared cooling, the surface below and space above being colder than the atmospheric layers where they form.

[11] Because clouds tend to be lower during the night than during the day, the daily averaged effect is a net cooling below 15 km and a net warming above. Figure 2a shows that the atmosphere is warmed by up to 9 K at ~20 km altitude in the afternoon and cooled by around 6 K below 10 km during the night. This nocturnal temperature inversion has been observed by the Radio Science instrument of MGS and explained in the light of the GCM simulations of *Hinson and Wilson* [2004]. These authors noted an intensification of the thermal tides by RAC. This intensification is also evident in Figure 2a, where the vertical propagation of the wavenumber one diurnal component is apparent in the temperature field (with a wavelength of about 30 km).

[12] To distinguish between radiative and dynamical responses, we performed single-column simulations in the same conditions as the GCM simulations, using the dust and water ice profiles extracted from the GCM simulation. In other words, Figure 2b is analogous to Figure 2a except that the dynamical responses are not modeled. A comparison of the two figures shows that during the night, thermal tides tend to increase temperature changes induced by RAC and have the opposite effect during the afternoon, which is consistent with the finding by *Hinson and Wilson* [2004]. Moreover, RAC increase daytime temperatures and favor vertical mixing of the dust layer, resulting in an indirect additional warming near 30 km altitude. This is demonstrated in Figure 2d, in which temperature change induced by vertical mixing of dust alone is represented. The direct radiative effect of clouds is shown in Figure 2c. Interestingly, we found that the temperature increase near the 30 km level is mainly due to the vertical redistribution of dust. For example, at 4 PM, dust mixing increases the temperature by ~9 K, versus 6 K for clouds (compare Figures 2d and 2c). Conversely nighttime cooling below the 10 km level is mainly caused by the radiative effect of clouds. Above the 10 km level, nighttime temperature is increased by dust redistribution first, and then by the radiative effect of clouds and the adiabatic heating of the thermal tides, the latter two each having an impact of around 3 K.

4. Three-Dimensional Simulations Including Radiatively Active Clouds (RAC)

[13] We now focus on the impact of RAC on the global thermal structure of the atmosphere using the LMD/MGCM, and compare the simulated temperatures with the ones measured by TES.

4.1. Global Temperature Changes Induced by Clouds

[14] Figures 3a–3d show the mean zonal temperature change induced by RAC for different periods of L_s, along with the zonal mean water ice mole mixing ratio in ppm (contours). Three main phenomena are occurring and detailed below.

[15] Near the equator, clouds tends to warm the atmosphere near the 0.5 hPa pressure level and to cool the atmosphere near 1 hPa. This is especially obvious at L_s = 0–30° (northern spring, see Figure 3a). This temperature pattern reflects the two processes described in section 3: a cooling of the lower atmosphere by nighttime emission of infrared radiation by clouds and a warming of the middle atmosphere by daytime absorption of surface infrared radiation. It is worth noting that after L_s = 150°, clouds still

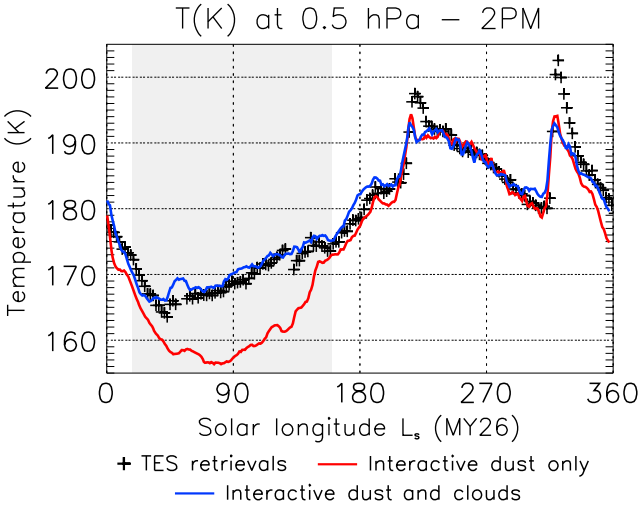

Figure 4. Equatorial temperature at 2 PM for the 0.5 hPa pressure level as measured by TES (+ crosses), and as predicted by the LMD/MGCM when using the semi-interactive dust scheme alone (red, same as in *Madeleine et al.* [2011, Figure 5a]) and when using both the semi-interactive dust scheme and the radiatively active water ice clouds (blue). The model predictions agree with the observations only when clouds are radiatively active, especially around L_s = 90° (shaded area).

warm the middle atmosphere in the equatorial regions by more than 10 K despite their low opacity (∼0.02 at 12.1 μm, see Figure 1).

[16] At the poles, low-lying clouds cool the atmosphere, especially at equinox, as clearly illustrated by Figures 3a and 3c. In the polar regions, the surface being colder than at lower latitudes because of reduced sunlight, the dominant process is the loss of infrared radiation to space, which cools the polar atmosphere by up to 20 K.

[17] In mid-latitudes, a warming is clearly apparent and is responsible for the inverted U-shaped temperature pattern apparent in Figure 3 at all seasons, especially for L_s = 90–120° (Figure 3b). This warming is not directly the result of the radiative effect of clouds, but is rather an indirect consequence of their effect. Indeed, clouds warm the middle atmosphere near the 0.5 hPa pressure level, thereby increasing the meridional temperature gradient. The meridional overturning circulation is intensified, and the adiabatic warming in the descending branch of the cell is increased. This effect is further illustrated by the gray lines in Figures 3b and 3d which represent the change in the meridional mass streamfunction due to RAC. The enhancement of the overturning circulation is evident and the Hadley cell provides twice as much transport than without RAC. The associated adiabatic warming in the descending branch of the Hadley cell is clearly apparent and can reach 20 K (see Figure 3b). Consequently, RAC do not only impact the surface and atmospheric temperatures where they form, but also have a profound indirect effect on the global dynamics of the atmosphere.

4.2. Comparison to the TES Observed Temperatures

[18] Figures 3e–3h show the temperature difference between LMD/MGCM predictions and TES retrievals when clouds are radiatively active. The three phenomena described in the previous section explain the remarkable improvements seen in Figure 3 (compare to the last column of Figure 4 in *Madeleine et al.* [2011]).

[19] GCM results are significantly improved in the equatorial regions where clouds tend to cool the lower atmosphere and warm the middle atmosphere. Without RAC, temperatures were respectively too warm and too cold in the two parts of the atmosphere. This is especially visible for the L_s = 90–120° period (Figure 3f). In the ±50° latitude band, GCMs were underestimating temperature by more than ∼10 K in the middle atmosphere when clouds were radiatively inactive [see *Wilson et al.*, 2008; *Madeleine et al.*, 2011]. This cold bias in GCM predictions almost disappears when clouds are radiatively active (Figure 3f).

[20] This improvement of the temperatures in the middle atmosphere is further illustrated in Figure 4. This figure shows daytime (2 PM) equatorial temperatures at the 0.5 hPa pressure level observed by TES (+ crosses) and simulated by the LMD/MGCM using two different configurations: with the semi-interactive dust scheme but without RAC in red and with both radiatively active dust and water ice clouds in blue (this figure is a follow-up of Figure 5a of *Madeleine et al.* [2011]). When clouds are radiatively active, temperatures are increased at almost all seasons and become consistent with the observations. This is especially obvious at the aphelion cloud season, during which the cold bias of ∼10 K disappears (shaded area in Figure 4). Temperatures in mid-latitudes are also improved as a result of the increased adiabatic warming in the descending branch of the Hadley cell. One last improvement noticeable in Figure 3 occurs at both poles where the temperature in the lower atmosphere is decreased by the loss of infrared radiation to space. This corrects a warm bias that was observed in simulations without RAC, but polar clouds are so thick that temperatures are now biased cold, as discussed in the next section.

4.3. Remaining Temperature Biases

[21] Some differences remain between model and observations mostly at high latitudes. For example, the lower atmosphere of the north polar region is too cold by ∼15 K during the L_s = 0–30° period (see Figure 3e). Later, between L_s = 90° and L_s = 120°, a warm bias occurs above 60° N near the 0.5 hPa pressure level. Interestingly, this warm bias can be explained by the effect of clouds forming at these altitudes (see Figures 3b and 3f). Hence, those clouds are probably thinner in reality than in the model, which might be due to the scavenging of dust nuclei by water ice clouds. In the winter hemisphere, a cold bias caused by clouds is also apparent in the lower atmosphere near 30°S (see Figure 3f). Similarly, for the L_s = 270–300° period, a cold bias of ∼16 K appears in the lower atmosphere at 30° N and is also caused by the radiative effect of clouds (see Figures 3d and 3h). Therefore, water ice clouds may not be well predicted in the polar regions at solsticial seasons in our model (see section 4.4). Finally, a cold bias remains near the 0.1 hPa pressure level during northern spring and summer (see Figure 3e and 3f). This might be due to an underestimation of the vertical extent of the tropical clouds, as pointed out by *Heavens et al.* [2010].

[22] It is worth noting that TES temperature retrievals are currently being refined using a new radiative transfer model [*Hoffman et al.*, 2011]. This new dataset modifies temperature in the polar regions and at the equator near the 0.1 hPa

pressure level. Therefore part of the biases seen in these regions of the atmosphere may also come from uncertainties in the TES temperature retrievals.

4.4. Impact of RAC on the Water Cycle

[23] RAC have a strong impact on the amount of water vapor that is provided by the north polar region. As mentioned earlier, clouds do not seem to be well predicted in the polar regions where we observe large temperature biases (see, e.g., Figures 3a and 3e). At the end of northern spring, during the L_s = 60–90° period, north polar clouds reflect sunlight and decrease the surface temperature of the permanent cap. Therefore, surface ice sublimation is reduced, and there is a global decrease in the amount of atmospheric water vapor. In the tropical regions, the resulting water vapor column is for example reduced by 5 to 10 pr.μm during summer. This departure from observations due to the inclusion of RAC is also found in other Mars GCMs, such as the NASA Ames MGCM [*Haberle et al.*, 2011]. It has motivated the development of a finer microphysics scheme in the LMD/MGCM to improve the prediction of cloud properties in the polar regions. The results of this new model are currently being analyzed [*Navarro et al.*, 2012].

5. Conclusions

[24] The radiative effect of clouds is a key component of the Martian climate system. Clouds do not only impact temperatures where they form by direct extinction of visible and infrared radiation, but also induce profound temperature changes in other regions of the planet by modifying the whole atmospheric circulation. Accounting for the radiative effect of clouds in the LMD/MGCM significantly improves temperature predictions. Now that the water cycle is fully coupled to the other components of the climate system, a whole new complexity arises. In particular, the sublimation of the polar ice deposits during northern summer is reduced when clouds are active, and the resulting amount of atmospheric water vapor departs from observations. Therefore, the water cycle is drawing renewed attention and further research is underway to better understand this emerging complexity. A better representation in the LMD/MGCM of cloud formation and interactions between the three main cycles of CO_2, dust and water should improve our results and will be the subject of future publications.

[25] **Acknowledgments.** Very helpful and constructive advice regarding the text was provided by an anonymous reviewer and John Wilson. We express our gratitude to Robin Wordsworth, Franck Montmessin, Anni Määttänen, and Michael Wolff for useful discussions. The LMD Mars GCM is developed with the support of Centre National de la Recherche Scientifique (CNRS), European Space Agency (ESA), and Centre National d'Études Spatiales (CNES) in collaboration with the AOPP (Atmospheric, Oceanic, and Planetary Physics laboratory, Oxford University) and IAA (Instituto de Astrofísica de Andalucía, Granada) groups. Grant support for this work was provided by the UPMC university through doctoral fellowship and by ESA and CNES. We would also like to acknowledge financial assistance from the NASA Mars Data Analysis Program grant NNX11AI81G to J. W. Head.

[26] The Editor thanks R. Wilson and an anonymous reviewer for their assistance in evaluating this paper.

References

Clancy, R. T., B. J. Sandor, M. J. Wolff, P. R. Christensen, M. D. Smith, J. C. Pearl, B. J. Conrath, and R. J. Wilson (2000), An intercomparison of ground-based millimeter, MGS TES, and Viking atmospheric temperature measurements: Seasonal and interannual variability of temperatures and dust loading in the global Mars atmosphere, *J. Geophys. Res.*, *105*, 9553–9571, doi:10.1029/1999JE001089.

Colaprete, A., O. B. Toon, and J. A. Magalhães (1999), Cloud formation under Mars Pathfinder conditions, *J. Geophys. Res.*, *104*, 9043–9053.

Conrath, B. J., J. C. Pearl, M. D. Smith, W. C. Maguire, P. R. Christensen, S. Dason, and M. S. Kaelberer (2000), Mars Global Surveyor Thermal Emission Spectrometer (TES) observations: Atmospheric temperatures during aerobraking and science phasing, *J. Geophys. Res.*, *105*, 9509–9519.

Haberle, R. M., M. M. Joshi, J. R. Murphy, J. R. Barnes, J. T. Schofield, G. Wilson, M. Lopez-Valverde, J. L. Hollingsworth, A. F. C. Bridger, and J. Schaeffer (1999), General circulation model simulations of the Mars Pathfinder atmospheric structure investigation/meteorology data, *J. Geophys. Res.*, *104*, 8957–8974.

Haberle, R. M., F. Montmessin, M. A. Kahre, J. L. Hollingsworth, J. Schaeffer, M. J. Wolff, and R. J. Wilson (2011), Radiative effects of water ice clouds on the Martian seasonal water cycle, in *Fourth International Workshop on the Mars Atmosphere: Modelling and Observations*, pp. 223–226, Lab. de Meteorol. Dyn., Paris.

Heavens, N. G., J. L. Benson, D. M. Kass, A. Kleinböhl, W. A. Abdou, D. J. McCleese, M. I. Richardson, J. T. Schofield, J. H. Shirley, and P. M. Wolkenberg (2010), Water ice clouds over the Martian tropics during northern summer, *Geophys. Res. Lett.*, *37*, L18202, doi:10.1029/2010GL044610.

Hinson, D. P., and R. J. Wilson (2004), Temperature inversions, thermal tides, and water ice clouds in the Martian tropics, *J. Geophys. Res.*, *109*, E01002, doi:10.1029/2003JE002129.

Hoffman, M. J., J. Eluszkiewicz, R. Hoffman, S. J. Greybush, E. Kalnay, and R. J. Wilson (2011) Evaluation of an optimal spectral sampling retrieval algorithm for thermal emission spectrometer radiances, in *Fourth International Workshop on the Mars Atmosphere: Modelling and Observations*, pp. 41–43, Lab. de Meteorol. Dyn., Paris.

Madeleine, J.-B., F. Forget, E. Millour, L. Montabone, and M. J. Wolff (2011), Revisiting the radiative impact of dust on Mars using the LMD Global Climate Model, *J. Geophys. Res.*, *116*, E11010, doi:10.1029/2011JE003855.

Madeleine, J.-B., et al. (2012), Aphelion water-ice cloud mapping and property retrieval using the OMEGA imaging spectrometer onboard Mars Express, *J. Geophys. Res.*, *117*, E00J07, doi:10.1029/2011JE003940.

Magalhães, J. A., J. T. Schofield, and A. Seiff (1999), Results of the Mars Pathfinder atmospheric structure investigation, *J. Geophys. Res.*, *104*, 8943–8951.

Montabone, L., S. R. Lewis, P. L. Read, and D. P. Hinson (2006), Validation of Martian meteorological data assimilation for MGS/TES using radio occultation measurements, *Icarus*, *185*, 113–132.

Montmessin, F., F. Forget, P. Rannou, M. Cabane, and R. M. Haberle (2004), Origin and role of water ice clouds in the Martian water cycle as inferred from a general circulation model, *J. Geophys. Res.*, *109*, E10004, doi:10.1029/2004JE002284.

Navarro, T., F. Forget, E. Millour, A. Spiga, A. Colaitis, J.-B. Madeleine, F. Montmessin, and A. Määttänen (2012), An improved climate model for the LMD global climate model: Application to Mars climate now and in the past thousand years, paper presented at the Mars Recent Climate Change Workshop, NASA Ames Mars Clim Model. Group, Moffett Field, Calif., 15–17 May.

Rodin, A. V., R. J. Wilson, R. T. Clancy, and M. I. Richardson (1999), The coupled roles of dust and water ice clouds in the Mars aphelion season, in *The Fifth International Conference on Mars*, p. 6235, Lunar Planet. Inst., Houston, Tex.

Schofield, J. T., J. R. Barnes, D. Crisp, R. M. Haberle, S. Larsen, J. A. Magalhães, J. R. Murphy, A. Seiff, and G. Wilson (1997), The Mars Pathfinder atmospheric structure investigation/meteorology (ASI/MET) experiment, *Science*, *278*, 1752–1758.

Smith, M. D. (2004), Interannual variability in TES atmospheric observations of Mars during 1999–2003, *Icarus*, *167*, 148–165.

Warren, S. G. (1984), Optical constants of ice from the ultraviolet to the microwave, *Appl. Opt.*, *23*(8), 1206–1225.

Wilson, R. J. (2011), Water ice clouds and thermal structure in the Martian tropics as revealed by Mars Climate Sounder, in *Fourth International Workshop on the Mars Atmosphere: Modelling and Observations*, pp. 219–222, Lab. de Meteorol. Dyn., Paris.

Wilson, R. J., G. A. Neumann, and M. D. Smith (2007), Diurnal variation and radiative influence of Martian water ice clouds, *Geophys. Res. Lett.*, *34*, L02710, doi:10.1029/2006GL027976.

Wilson, R. J., S. R. Lewis, L. Montabone, and M. D. Smith (2008), Influence of water ice clouds on Martian tropical atmospheric temperatures, *Geophys. Res. Lett.*, *35*, L07202, doi:10.1029/2007GL032405.

Withers, P., and M. D. Smith (2006), Atmospheric entry profiles from the Mars Exploration Rovers Spirit and Opportunity, *Icarus*, *185*, 133–142.

Wolff, M. J. and R. T. Clancy (2003), Constraints on the size of Martian aerosols from Thermal Emission Spectrometer observations, *J. Geophys. Res.*, *108*(E9), 5097, doi:10.1029/2003JE002057.